9416 *Biochemistry* **2009,** *48,* 9416–9426
DOI: 10.1021/bi901221s

BIOCHEMISTRY
including biophysical chemistry & molecular biology
Article

Thiol and Sulfenic Acid Oxidation of AhpE, the One-Cysteine Peroxiredoxin from *Mycobacterium tuberculosis*: Kinetics, Acidity Constants, and Conformational Dynamics[†]

Martín Hugo,[‡,§] Lucía Turell,[§,∥] Bruno Manta,[§,⊥] Horacio Botti,[§,⊥] Gisele Monteiro,[#] Luis E. S. Netto,[#] Beatriz Alvarez,[§,∥] Rafael Radi,[‡,§] and Madia Trujillo*[,‡,§]

[‡]*Departamento de Bioquímica, Facultad de Medicina,* [§]*Center for Free Radical and Biomedical Research, Facultad de Medicina and*[∥] *Instituto de Química Biológica, Facultad de Ciencias, Universidad de la República, Montevideo, Uruguay,* [⊥]*Institut Pasteur de Montevideo, Montevideo, Uruguay, and* [#]*Departamento de Biologia, Instituto de Biociências, Universidade de São Paulo, São Paulo, Brazil*

Received July 16, 2009; Revised Manuscript Received September 5, 2009

ABSTRACT: Drug resistance and virulence of *Mycobacterium tuberculosis* are partially related to the pathogen's antioxidant systems. Peroxide detoxification in this bacterium is achieved by the heme-containing catalase peroxidase and different two-cysteine peroxiredoxins. *M. tuberculosis* genome also codifies for a putative one-cysteine peroxiredoxin, alkyl hydroperoxide reductase E (*Mt*AhpE). Its expression was previously demonstrated at a transcriptional level, and the crystallographic structure of the recombinant protein was resolved under reduced and oxidized states. Herein, we report that the conformation of *Mt*AhpE changed depending on its single cysteine redox state, as reflected by different tryptophan fluorescence properties and changes in quaternary structure. Dynamics of fluorescence changes, complemented by competition kinetic assays, were used to perform protein functional studies. *Mt*AhpE reduced peroxynitrite 2 orders of magnitude faster than hydrogen peroxide (1.9×10^7 M^{-1} s^{-1} vs 8.2×10^4 M^{-1} s^{-1} at pH 7.4 and 25 °C, respectively). The latter also caused cysteine overoxidation to sulfinic acid, but at much slower rate constant (40 M^{-1} s^{-1}). The pK_a of the thiol in the reduced enzyme was 5.2, more than one unit lower than that of the sulfenic acid in the oxidized enzyme. The pH profile of hydrogen peroxide-mediated thiol and sulfenic acid oxidations indicated thiolate and sulfenate as the reacting species. The formation of sulfenic acid as well as the catalytic peroxidase activity of *Mt*AhpE was demonstrated using the artificial reducing substrate thionitrobenzoate. Taken together, our results indicate that *Mt*AhpE is a relevant component in the antioxidant repertoire of *M. tuberculosis* probably involved in peroxide and specially peroxynitrite detoxification.

Tuberculosis (TB)[1] is a serious, often lethal infectious disease caused by *Mycobacterium tuberculosis*, which affects about one-third of the human population. Multidrug resistance TB is an emerging problem of great public health concern worldwide, making new drug development a priority (*1*). This bacterium is able to live and proliferate within the phagosomes of activated macrophages, where it is exposed to a strong oxidative stress (*2*) that includes hydrogen peroxide (H_2O_2) and peroxynitrite[2] production. Reactive oxygen and nitrogen species are cytotoxic (*3*−*5*), and several lines of evidence indicate their role in the control of *M. tuberculosis* infection (*5*−*7*). Thus, the mechanisms that allow the pathogen to cope with these species constitute an active field of investigation (*2*, *8*, *9*).

The antioxidant defense in *M. tuberculosis* is unusual in many aspects. While *M. tuberculosis* lacks the typical glutathione system, it contains millimolar concentrations of mycothiol [2-(*N*-acetylcysteinyl)amido-2-deoxy-α-D-glucopyranosylmyoinositol](*10*), mycothiol reductase (*11*), and different thiol disulfide oxidoreductases (*12*, *13*). It also contains catalase peroxidase, a heme-dependent peroxidase that reduces different peroxides including peroxynitrite, and is responsible for the activation of the first line antituberculosis prodrug isoniazid (*14*, *15*). As expected, mutations of *katG* result in resistance to this drug (*16*), and interestingly, infective forms of *katG* mutants show increased expression of alkyl hydroperoxide reductase C (AhpC) (*17*), a member of the peroxiredoxin (Prx) family. *M. tuberculosis* also expresses thioredoxin peroxidase (TPx), another two-Cys Prx, which is known to react rapidly with peroxynitrite (*9*) and has been recently proved to be an important virulence factor in cellular and animal models of TB (*18*). In addition, *M. tuberculosis* genome codifies for three other Prxs (*19*). Among them, the hypothetical bacterioferritin comigratory proteins have proved to be important for survival under oxidative stress conditions in other organisms (*20*, *21*). Finally, a gene for a putative one-Cys Prx, alkyl hydroperoxide reductase E (AhpE, annotated as Rv2238c), has also been identified in *M.*

[†]This work was supported by grants from Programa de Desarrollo Tecnológico (PDT 079), Ministerio de Educación y Cultura, Uruguay, to M.T. and B.A., from Howard Hughes Medical Institute and International Centre of Genetic Engineering and Biotechnology to R.R., and from FAPESP and INCT de Processos Redox em Biomedicina, Brazil, to L.E.S.N. and G.M. M.H., B.M., L.T., and H.B. were supported by fellowships from PEDECIBA-ANII, Uruguay.

*To whom correspondence should be addressed. E-mail: madiat@fmed.edu.uy. Telephone: (5982)9249561. Fax: (5982)9249563.

[1]Abbreviations: TB, tuberculosis; C_P, peroxidatic cysteine; DTNB, 5,5′-dithiobis(2-nitrobenzoate); dtpa, diethylenetriaminepentaacetic acid; DTT, dithiothreitol; GSH, glutathione; HRP, horseradish peroxidase; LiP, lignine peroxidase; *Mt*AhpE, *Mycobacterium tuberculosis* alkyl hydroperoxide reductase E; NAC, *N*-acetylcysteine; NEM, *N*-ethylmaleimide; Prx, peroxiredoxin; TNB, 5-thio-2-nitrobenzoate.

[2]The term peroxynitrite is used to refer to the sum of peroxynitrite anion ($ONOO^-$) and peroxynitrous acid (ONOOH) unless specified. IUPAC recommended names for $ONOO^-$ and ONOOH are oxoperoxonitrate(1−) and hydrogen oxoperoxonitrate, respectively.

 Published on Web 09/08/2009

tuberculsosis and is highly conserved among many other Mycobacteria (*19*, *22*). The regulated expression of *Mt*AhpE has been reported at a transcriptional level (*23*), and the crystallographic structures of the recombinant protein under reduced and oxidized states have been determined (*24*). In solution, the enzyme was reported to be present as a mixture of dimeric and octameric forms, but redox state-dependent changes in its quaternary structure, as observed for other Prxs (*25*), have not been previously investigated. The functional properties of *Mt*AhpE have not been addressed so far. MtAhpE protein contains a single cysteine residue (Cys45) that is predicted to be the peroxidatic cysteine (C_P), since it is located in a typical **P**XXX**T**XX**C** motif, well conserved in the amino acidic sequence of Prx active sites. Moreover, structural data on the recombinant enzyme show that an arginine residue (Arg116) interacts by hydrogen bonding with Cys45 (~3.5 Å distant) allowing thiolate stabilization, another conserved feature among different Prxs (*26*).

During the oxidative part of the catalytic cycle of Prxs the thiolate in C_P (Prx-S^-) reduces peroxide substrates such as hydrogen peroxide (H_2O_2), peroxynitrous acid (ONOOH), or organic peroxides (ROOH) to water, nitrite, or alcohols (ROH), respectively, in a two-electron oxidation process that leads to sulfenic acid (Prx-SOH) formation:

$$\text{Prx-S}^- + \begin{matrix}\text{H}_2\text{O}_2\\ \text{ONOOH}\\ \text{ROOH}\end{matrix} \rightarrow \text{Prx-SOH} + \begin{matrix}\text{HO}^-\\ \text{NO}_2{}^-\\ \text{RO}^-\end{matrix} \quad (1)$$

In the crystal structure of the oxidized form of *Mt*AhpE, Cys45 was oxidized to a stable sulfenic acid (*24*), as previously reported for the human one-Cys Prx (*27*). In contrast to most two-Cys Prxs (*28*), the reducing step of one-Cys Prxs is still unclear (*29*−*33*).

Alternatively, and in the presence of high peroxide concentrations, sulfenic acid in Prxs can be overoxidized to sulfinic acid (Prx-SO_2H), through the reaction with a second molecule of oxidizing substrate, in a process that results in enzyme inactivation.

$$\text{Prx-SOH} + \text{ROOH} \rightarrow \text{Prx-SO}_2\text{H} + \text{ROH} \quad (2)$$

Overoxidation of the mammalian one-Cys Prx has been detected in cellular systems (*34*). There is just one estimation for the second-order rate constant of the reaction in eq 2, which is related to mammalian Prx 1 overoxidation by H_2O_2 (57 M^{-1} s^{-1} at physiological pH (*35*) estimated from ref *36*). The mechanism of the reaction, including the reacting species (RSO^- vs RSOH) as well as the pK_a of Prx sulfenic acids, which may affect the rate of the reaction at physiological pH, is far from being resolved.

In this work we demonstrate the peroxidatic activity of the putative one-cysteine Prx of *M. tuberculosis*, AhpE. Taking advantage of the different intrinsic fluorescence properties of this enzyme at its different redox states, or by using competition kinetic approaches, we investigated the enzymatic selectivity toward the main peroxide substrates the bacterium may encounter during infection. We performed mechanistic and kinetic studies on enzymatic overoxidation. The pK_a values of the thiol in the reduced enzyme as well as that of the sulfenic acid in the oxidized enzyme were determined. The results obtained add to our knowledge of the peroxide detoxification mechanisms in *M. tuberculosis*, an important issue for understanding the biology of this extremely successful human pathogen.

MATERIALS AND METHODS

Chemicals. Horseradish peroxidase (HRP) and lignine peroxidase (LiP) were obtained from Sigma and Fluka, respectively. Argon (99.5% pure) was from AGA Gas Co., Montevideo, Uruguay. H_2O_2 was from Mallinckrodt Chemicals. Peroxynitrite was synthesized from H_2O_2 and nitrous acid as described previously (*37*, *38*). Treatment of a stock solution of peroxynitrite with granular manganese dioxide eliminated H_2O_2 remaining from the synthesis. Nitrite contamination was typically less than 30% of peroxynitrite concentration. 5-Thio-2-nitrobenzoate (TNB) free of its disulfide, 5,5′-dithiobis(2-nitrobenzoate) (DTNB), was synthesized as previously described (*39*). All other reagents were obtained from standard commercial sources and used as received.

All experiments were performed in 100 mM sodium phosphate buffer containing 0.1 mM diethylenetriaminepentaacetic acid (dtpa), pH 7.4 and 25 °C, unless otherwise indicated.

Protein Expression and Purification. *Mt*AhpE (TB Database gene name Rv2238c) was expressed in *Escherichia coli* BL21(DE3) (expression vector pDEST17) as a recombinant His-tagged protein and purified as previously described (*24*). The *Mt*AhpE mutant C45S was generated by site-directed mutagenesis using the QuikChange site-directed mutagenesis kit (Stratagene) as described by the manufacturer (previously reported in ref *31*) using the following primers: C45Sfw, 5′ CAC GGG CAT CTC ACA GGG CGA GC 3′; C45Srev, 5′ GCT CGC CCT GTG AGA TGC CCG TG 3′.

Peroxide, Protein, and Thiol Quantitation. The concentration of H_2O_2 stock solutions was measured at 240 nm (ε_{240} = 43.6 M^{-1} cm^{-1}) (*40*). Peroxynitrite concentration was determined at alkaline pH at 302 nm (ε_{302} = 1670 M^{-1} cm^{-1}) (*38*). *Mt*AhpE concentration was determined spectrophotometrically at 280 nm, using a molar absorption coefficient of 23950 M^{-1} cm^{-1} calculated according to ref *41*, that was in good agreement with protein measurements by the biuret assay (not shown). Protein thiol content was measured by Ellman's assay (ε_{412} = 14150 M^{-1} cm^{-1}). Recently purified *Mt*AhpE typically contained ~0.9 thiol/protein, and thiol content diminished with storage (under argon atmosphere, at −80 °C).[3] The concentrations of HRP and LiP were determined by their absorption at the Soret band (ε_{403} = 1.02×10^5 M^{-1} cm^{-1} (*42*) and ε_{409} = 1.68×10^5 M^{-1} cm^{-1} (*43*), respectively).

Protein Thiol Reduction and Alkylation. *Mt*AhpE was reduced immediately before use by incubation with 1 mM DTT for 30 min at 4 °C. Excess reductant was removed either by gel filtration using a HiTrap column (Amersham Bioscience) and UV−vis detection at 280 nm or, when using small volumes (< 200 μL), by passing the enzyme twice through Microbiospin 6 chromatography columns (Bio-Rad). Samples were extensively purged with argon once collected. For protein thiol alkylation, previously reduced *Mt*AhpE was incubated with *N*-ethylmaleimide (NEM) (5 or 10 mM) for 30 min at 4 °C, and excess NEM was removed as described for DTT.

Changes in the Intrinsic Fluorescence Intensity of MtAhpE. Emission spectra (λ_{exc} = 280 or 295 nm) of wild-type or C45S enzyme (1.5 μM) were obtained using an Aminco Bowman Series 2 luminescence spectrophotometer.

Size-Exclusion Chromatography. *Mt*AhpE (250 μL, 0.1 mg of protein) under different redox states was resolved on a Superdex 75 10/300 column, preequilibrated with phosphate buffer (20 mM, 150 mM NaCl, pH 7.4), with UV detection

[3]Due to the rapid reaction of oxidized *Mt*AhpE with TNB (see below), that could result in thiol content underestimation, thiol quantitations were performed in prereduced enzyme or in recently purified enzyme.

at 215 and 280 nm and a flow rate of 0.5 mL/min at 25 °C. The column was calibrated with molecular weight standards (Sigma-Aldrich).

Electrophoretic Analysis of MtAhpE. SDS−PAGE electrophoresis of reduced and oxidized enzyme under nonreducing conditions was performed using 13% acrylamide gels (0.2 μg of protein per well) that were silver stained for protein detection.

Electrospray Ionization Mass Spectrometry (ESI-MS) analysis. Freshly purified enzyme was incubated with the indicated concentrations of NEM (during 30 min), DTT or H_2O_2 (during 2 min), or H_2O_2 (during 1 min) followed by DTT, *N*-acetylcysteine (NAC), or glutathione (GSH) addition for 2 minutes in the above-mentioned buffer, pH 7.4 and 25 °C. Samples were passed twice through Microbiospin 6 columns equilibrated with H_2O, diluted into 1:1 acetonitrile:H_2O, 0.1% acetic acid, pH 4.5, to a final concentration of 1 μM and loaded into a QTRAP 2000 mass spectrometer (Applied Biosystems/MDS Sciex). Positive ion ESI mass spectra were collected using an m/z range of 700−1700, with ion spray voltage (IS) 5000 V, declustering potential (DP) 60 V, and entrance potential (EP) 10 V. Data acquisition was set to 3 min, and the final mass of *Mt*AhpE was calculated by automatic deconvolution using Analyst 1.4 software.

Kinetics of MtAhpE Oxidation and Overoxidation Studied Using a Direct Fluorometric Approach. The rate constants of *Mt*AhpE oxidation by H_2O_2 and peroxynitrite (eq 1) were determined by taking advantage of the decrease in protein intrinsic fluorescence intensity (λ_{exc} = 280 nm) that occurred upon oxidation. Reduced, NEM-blocked wild-type *Mt*AhpE or the C45S mutant (*Mt*AhpEC45S) was rapidly mixed with either peroxynitrite or H_2O_2 in excess in an Applied Photophysics SX-17MV stopped-flow spectrophotometer with a mixing time of <2 ms. Although peroxynitrite is an unstable species, it decays with a first-order rate constant of 0.27 s^{-1} at pH 7.4 and 25 °C, much slower than the reaction with *Mt*AhpE, so that pseudo-first-order conditions are maintained over the time course of the reaction (<0.1 s). Observed rate constants of fluorescence decrease (k_{obs}) were determined by fitting stopped-flow data to single exponential functions. Second-order rate constants for the reaction between prereduced enzyme and peroxynitrite or H_2O_2 were obtained from the slope of the plot of k_{obs} versus oxidant concentration.

For the determination of the rate constant of oxidized *Mt*AhpE overoxidation by H_2O_2 (eq 2), we took advantage of the increase in the enzyme intrinsic fluorescence intensity that occurred when it was treated with a large excess of H_2O_2. Reduced or NEM-blocked wild-type *Mt*AhpE (1 μM) was mixed with H_2O_2 (100−450 μM) in an Aminco Bowman Series 2 luminescence spectrophotometer, and time courses of fluorescence intensity change (λ_{exc} = 295 nm, λ_{em} = 338 nm) were registered. Second-order rate constants were obtained as described above for enzyme oxidation.

The pK_a of both the peroxidatic thiol group in reduced *Mt*AhpE and the sulfenic acid in oxidized *Mt*AhpE were measured by determining the rate constants of H_2O_2-mediated *Mt*AhpE C_P oxidation and overoxidation (eqs 1 and 2, respectively) at different pH values. Buffer systems used were sodium phosphate, 100 mM, plus 0.1 mM dtpa (pH 5.8−7.8) or sodium acetate buffer, 100 mM, plus 0.1 mM dtpa (pH < 5.8), with NaCl additions so as to keep ionic strength constant. When analyzing the effect of pH on overoxidation, the reduced enzyme was previously oxidized to sulfenic acid by treatment with an equimolar amount of H_2O_2 for 2 min at pH 7.4, 25 °C, and then exposed to excess H_2O_2 at the pH of interest. Rate constants for oxidation and overoxidation (k_{app}) were plotted against pH and fitted to

$$k_{app} = k_2 \frac{K_{AH}}{K_{AH} + [H^+]} \quad (3)$$

where k_{app} is the observed rate constant for *Mt*AhpE thiol oxidation ($k_{AhpE\text{-}S^-app}$) or overoxidation ($k_{AhpE\text{-}SO^-app}$) at a given pH value, k_2 represents the maximum rate constants for the reactions at alkaline pH, i.e., the pH-independent rate constants, and K_{AH} is the equilibrium constant for the deprotonation processes, where AH represents either the peroxidatic thiol or the sulfenic acid intermediate.

Kinetics of MtAhpE Oxidation Studied by a Competition Approach. The second-order rate constants for the reactions between reduced *Mt*AhpE and H_2O_2 or peroxynitrite were also determined by competition assays as reported previously (*44*−*47*). HRP was used to determine the rate constant for the reaction between *Mt*AhpE and peroxynitrite, whereas LiP was used for determining that between *Mt*AhpE and H_2O_2. In both cases, the reactions were followed using an Applied Photophysics SX-17MV stopped-flow spectrophotometer.

In the case of peroxynitrite-mediated HRP oxidation, the reaction was followed at 398 nm and HRP-compound I concentration was measured using a $\Delta\varepsilon_{398} = 4.2 \times 10^4$ M^{-1} cm^{-1} (*48*). The rate constant of peroxynitrite-mediated HRP oxidation to compound I was determined as 3×10^6 M^{-1} s^{-1} under the experimental conditions employed herein (data not shown) in agreement with previously published data (*49*). The rate constant of peroxynitrite-mediated *Mt*AhpE oxidation was calculated as previously (*44*−*47*).

In the case of H_2O_2-mediated LiP oxidation, the reaction was followed at 401 nm (isosbestic point for LiP-compound I and II determined by us; data not shown), and LiP-compound I concentration was determined assuming an equimolar reaction with H_2O_2. The rate constant for H_2O_2-mediated LiP oxidation to compound I was measured as 6.5×10^5 M^{-1} s^{-1} at pH 7.4 and 25 °C (data not shown), in agreement with previously reported values (*43*). The rate constant of H_2O_2-mediated *Mt*AhpE oxidation was calculated as above.

Computer-assisted simulations were performed using GEPASI 3 program (*50*, *51*).

Kinetics of MtAhpE Reaction with TNB and DTNB. The reactions were studied using a Varian Cary 50 spectrophotometer with a stopped-flow accessory (Applied Photophysics RX 2000). Thionitrobenzoate has been previously used to quantify sulfenic acid formed in one-Cys Prxs and human serum albumin upon oxidation (*39*, *52*). Herein, the kinetics of *Mt*AhpE reduction by TNB was studied by mixing increasing concentrations of reduced *Mt*AhpE (0.5−2.5 μM) and TNB (74 μM) in one syringe with H_2O_2 (20 μM) in the other syringe, at pH 7.4 and 25 °C, and recording TNB absorbance at 412 nm. The rate constant of reduced *Mt*AhpE oxidation by DTNB was determined by measuring initial rates of TNB formation from the reaction between reduced *Mt*AhpE (6 μM) with DTNB (100−500 μM) at pH 7.4 and 25 °C.

RESULTS

MtAhpE Oxidation and Overoxidation Are Accompanied by Significant Structural Changes. (*A*) *Changes on MtAhpE*

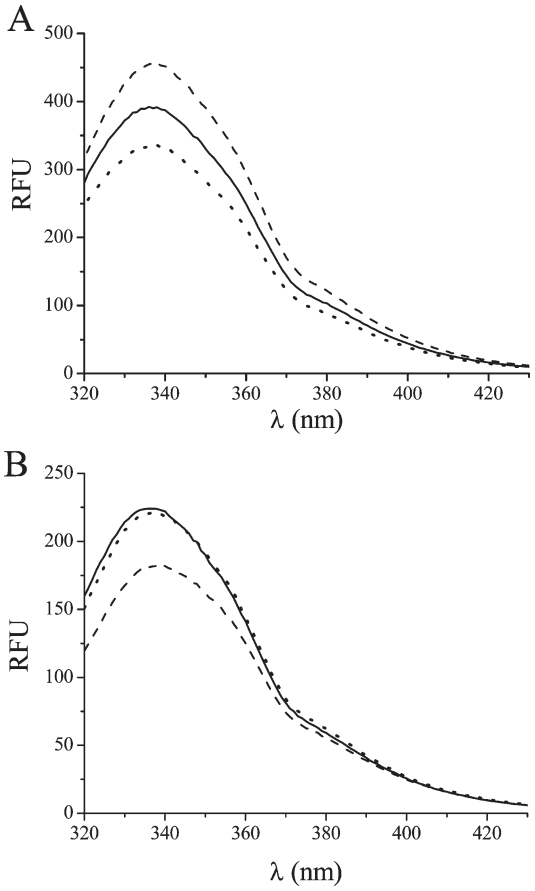

FIGURE 1: Intrinsic fluorescence of *Mt*AhpE under different redox states. (A) Fluorescence emission spectra (λ_{ex} = 295 nm) of *Mt*AhpE (1.5 μM, 0.83 μM thiol) without any further addition (solid line), plus 0.85 μM H_2O_2 (dotted line), and plus 1 mM DTT (dashed line). (B) Prereduced *Mt*AhpE (1.0 μM) without any further addition (solid line) or after addition of 300 μM H_2O_2 for 1 min (dashed line) or 10 min (dotted line).

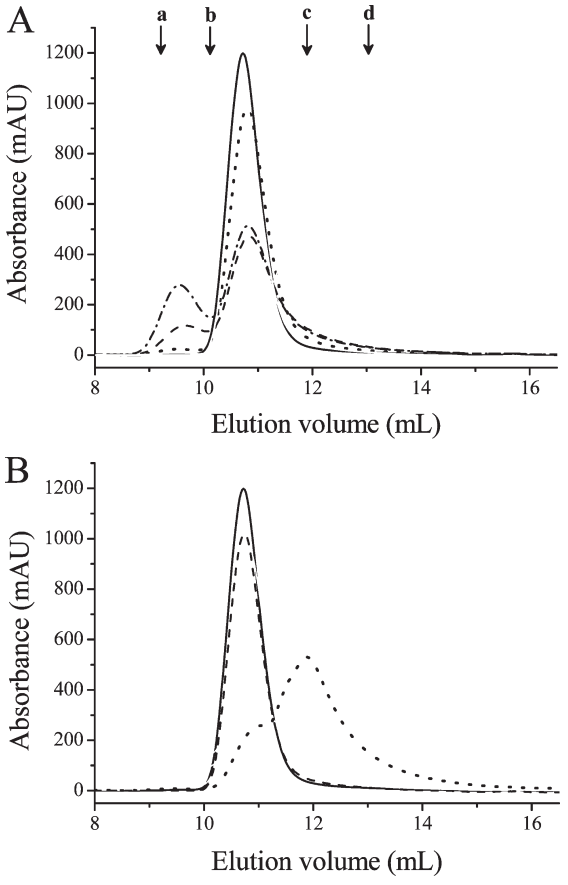

FIGURE 2: Redox-mediated changes in quaternary structure of *Mt*AhpE. (A) Elution profiles of *Mt*AhpE on a Superdex 75 10/300 column. *Mt*AhpE (0.1 mg) was loaded onto a column previously equilibrated with 20 mM phosphate buffer, and 150 mM NaCl, pH 7.4, with no previous treatment (solid line), upon incubation with equimolar H_2O_2 (1 min, dashed line; 60 min, dashed-dotted line), and after addition of a 20-fold excess of H_2O_2 (10 min, dotted line). Arrows indicate the position of molecular mass calibrants: from a to d, 67, 43, 25, and 13.7 kDa. (B) Solid line, the same as in (A) after treatment with equimolar amounts of H_2O_2 for 60 min and with further addition of 1 mM DTT (dashed line) or 2 mM *N*-acetylcysteine (dotted line).

Fluorescence Intensity. When recombinant His-tagged *Mt*AhpE (1.5 μM) was exposed to H_2O_2 (0.85 μM), an important decrease in the intrinsic fluorescence intensity was observed (Figure 1A). This change was reverted by reduction with DTT (1 mM), which recovered intensities to even higher levels than initially (Figure 1A). This is in agreement with the fact that the enzyme used had been stored for some days and was only partially reduced. No change in the fluorescence intensity was observed when either reduced *Mt*AhpE previously treated with NEM or *Mt*AhpEC45S was exposed to the same treatments (not shown). These data confirm that the oxidation of the peroxidatic (and single) cysteine of *Mt*AhpE is required for the observed fluorescence intensity changes. Moreover, when prereduced *Mt*AhpE (1 μM) was treated with a large excess of H_2O_2 (300 μM), there was an initial fast decrease followed by a slower increase in protein fluorescence intensity (Figure 1B). Again, these changes were precluded by pretreatment of the enzyme with NEM in excess (not shown), indicating the participation of the cysteine residue in the process, and supporting that H_2O_2-dependent overoxidation of the sulfenic acid of the oxidized enzyme (C_P-SOH) to sulfinic acid (C_P-SO_2H) was responsible for the fluorescence recovery (see below).

(*B*) *MtAhpE Quaternary Structure Is Dependent on Its Oxidation State*. Reduced *Mt*AhpE migrated as a monomer, and only a slight fraction of oxidized enzyme formed intramolecular disulfides when analyzed by nonreducing SDS−PAGE electrophoresis (not shown). In size exclusion chromatography, reduced enzyme (60 μM) eluted as a unique peak with an elution volume corresponding to a dimer (Figure 2A, solid line). Oxidation of the enzyme with an equimolar amount of H_2O_2 resulted in the slow formation of higher molecular weight species, while addition of excess H_2O_2 to promote enzyme overoxidation resulted again in a dimeric form (Figure 2A). The higher molecular weight species formed after incubation with equimolar H_2O_2 were reversed by the addition of 1 mM DTT (Figure 2B). Interestingly, addition of 1 mM *N*-acetylcysteine (NAC; low molecular weight thiol that can be formed from mycothiol enzymatic degradation in *M. tuberculosis* (*53*)) to *Mt*AhpE treated with equimolar H_2O_2 resulted in a destabilization of the dimer, leading to lower molecular weight species (Figure 2B). This could be due to the formation of a mixed disulfide through the reaction between the cysteine sulfenic acid (C_P-SOH) in oxidized *Mt*AhpE and the thiol group of NAC, as confirmed by mass spectrometry (see below). These results show that the quaternary structure of the protein is tightly controlled by the redox state of the peroxidatic cysteine.

Mass Spectrometry Analysis of Cysteine Modifications in MtAhpE. Recently purified enzyme without further additions displayed a molecular mass of 19319 Da (Figure 3A).When

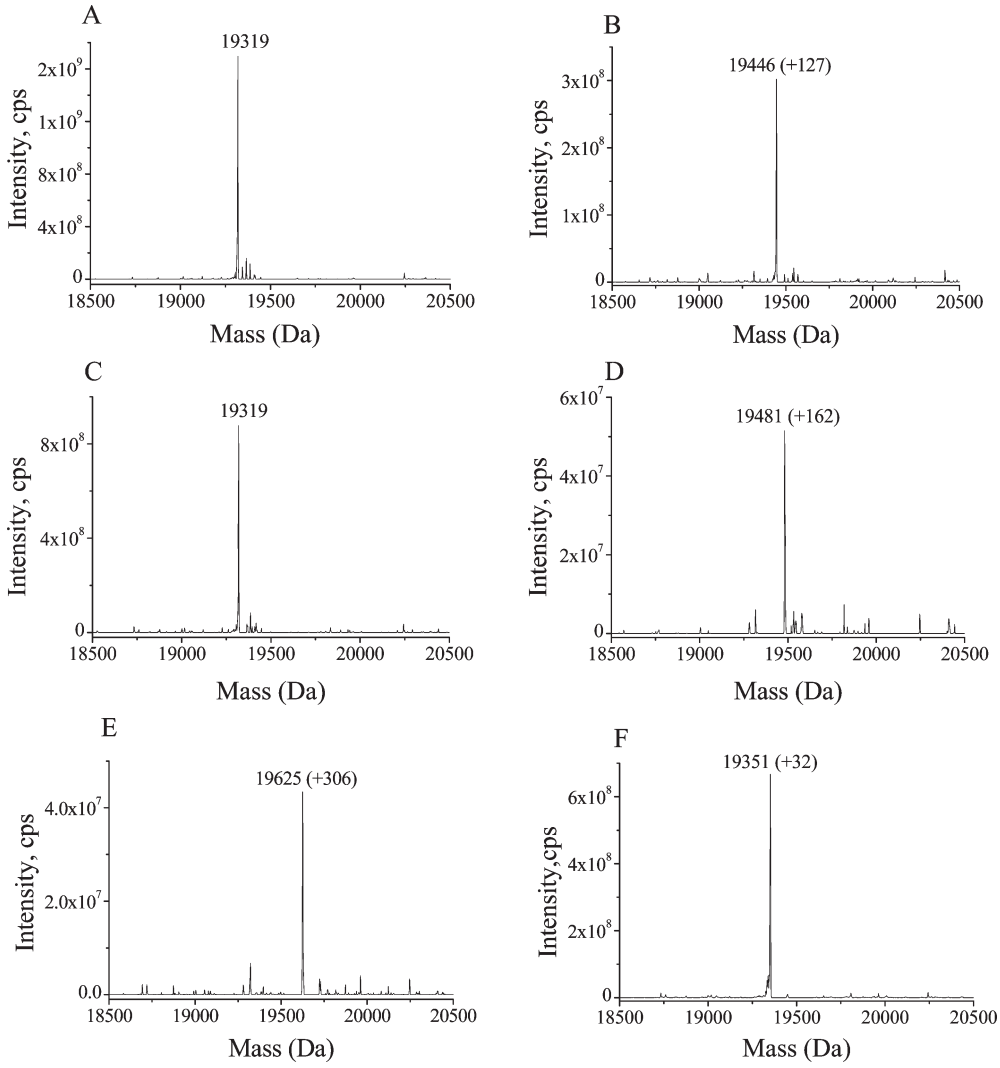

FIGURE 3: Covalent modifications of the *Mt*AhpE cysteine residue. Electrospray ionization mass spectrometry analysis of *Mt*AhpE (50 μM) with no further treatment (A), incubated with 5 mM NEM during 30 min (B), oxidized with equimolar H_2O_2 for 1 min and then treated with either 1 mM DTT (C), 2 mM NAC (D), or 2 mM GSH (E), and treated with excess H_2O_2 (250 μM) during 2 min (F). Samples were desalted and diluted to 1 μM concentration for mass spectrometric analysis.

*Mt*AhpE (50 μM) was incubated with excess NEM (5 mM during 30 min), the observed shift in molecular weight was consistent with the complete alkylation of C_P, indicating a $k > 0.5\ M^{-1}\ s^{-1}$ for the reaction at pH 7.4 and 25 °C (Figure 3B). Upon oxidation of *Mt*AhpE (50 μM) with equimolar H_2O_2 we were unable to detect the free sulfenic acid form of the enzyme. In the search for potential traps for sulfenic acid in oxidized *Mt*AhpE, the enzyme was exposed to equimolar H_2O_2 and 2 min later, it was incubated with excess DTT, NAC, or GSH. In the first case, a peak of 19319 Da was observed (Figure 3C), corresponding to the reduced enzyme. Incubation with NAC or GSH caused a mass shift of +162 and +306, respectively (Figure 3D,E), due to the formation of mixed disulfides with the oxidized enzyme. Finally, upon exposure of the enzyme (50 μM) to excess H_2O_2 (250 μM) for 2 min, a mass increment of 32 Da was detected, consistent with the addition of two oxygen atoms (Figure 3F).

Kinetics of Enzyme Oxidation by Peroxynitrite. (*A*) *Direct Approach Determinations*. Addition of increasing concentrations of excess peroxynitrite led to a dose-dependent increase in the observed rate constants of *Mt*AhpE intrinsic fluorescence change (Figure 4A, line a and inset). Changes were not observed when the C45S mutated enzyme was used (Figure 4A, line b) or by mixing wild-type enzyme with peroxynitrite decomposition products (Figure 4A, line c). From the slope of the plot shown in Figure 4A inset, a second-order rate constant of $(1.9 \pm 0.2) \times 10^7\ M^{-1}\ s^{-1}$ at pH 7.4 and 25 °C was determined.

(*B*) *Competition Approach Measurements*. The reaction between reduced *Mt*AhpE and peroxynitrite was also studied by competition with HRP. As expected, increasing concentrations of *Mt*AhpE inhibited peroxynitrite-mediated HRP-compound I formation (Figure 4B, inset). From these data the second-order rate constant for peroxynitrite reduction by *Mt*AhpE was calculated as $(1.7 \pm 0.6) \times 10^7\ M^{-1}\ s^{-1}$ at pH 7.4 and 25 °C, in close agreement with the value obtained by the fluorescence approach. Total compound I formation at different *Mt*AhpE concentrations were consistent with yields expected according to computer-assisted simulations, assuming a simple competition system (Figure 4B).

Kinetics of Enzyme Oxidation by H_2O_2. (*A*) *Direct Approach Determinations*. Mixing with increasing concentrations of excess H_2O_2 led to a dose-dependent increase in the observed rate constants of *Mt*AhpE fluorescence intensity change (Figure 5A). The second-order rate constant of this reaction was determined as $(8.2 \pm 1.5) \times 10^4\ M^{-1}\ s^{-1}$ at pH 7.4 and 25 °C (Figure 5A, inset).

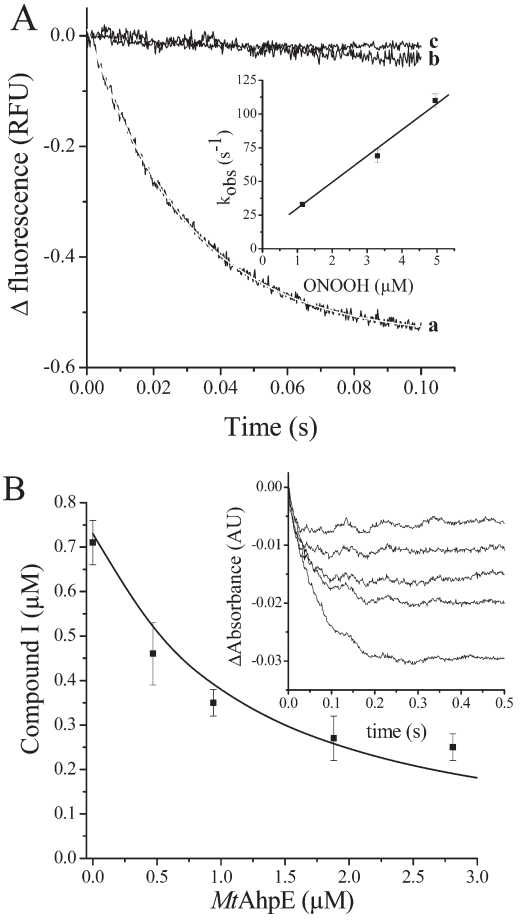

FIGURE 4: Kinetics of peroxynitrite-mediated *Mt*AhpE oxidation. (A) Prereduced wild-type (a) or C45S *Mt*AhpE (b) (0.25 μM) was rapidly mixed with peroxynitrite (1.15 and 3.3 μM, respectively) in sodium phosphate buffer, 100 mM, containing 0.1 mM dtpa, pH 7.4 and 25 °C, and the time-dependent decrease in total emission fluorescence intensity was determined. (c) As in (a) but using predecomposed peroxynitrite (3.3 μM). The gray trace represents the fit of experimental data in (a) to a single exponential function. Inset: Effect of increasing peroxynitrite concentrations on the observed rate constants (k_{obs}) of fluorescence change. (B) HRP (5 μM) was rapidly mixed with peroxynitrite (1.0 μM) in the presence of increasing concentrations of prereduced *Mt*AhpE. The concentration of compound I formed at each *Mt*AhpE concentration (squares) was determined. The continuous line represents the computer-assisted simulation of compound I yields according to a simple competition system using the calculated rate constant (k_2 = (1.7 ± 0.6) × 10^7 M^{-1} s^{-1}). Inset: Time courses of HRP oxidation by peroxynitrite in the presence of increasing reduced *Mt*AhpE concentrations (from bottom to top: 0, 0.47, 0.94, 1.9, and 2.8 μM).

Second-order rate constants for H_2O_2-mediated *Mt*AhpE oxidation were faster at alkaline pHs (Figure 5B), indicating that thiolate in C_P was the reacting species, in agreement with previously proposed mechanism of reaction (*54*, *55*). *Mt*AhpE was unstable and precipitated under low pH conditions (data not shown), thus limiting the pH range of our studies (pH >4.5). Amplitudes of fluorescence change decreased at acidic pH, but still k_{obs} values linearly depended on oxidant concentration. The pK_a of the peroxidatic thiol was estimated as 5.2. This is, to our knowledge, the first pK_a value reported for a 1-Cys Prx.

(*B*) *Competition Approach Measurements*. In order to confirm the value for k_2 for H_2O_2-mediated *Mt*AhpE oxidation obtained above, the reaction was also studied by a competition approach (*44*, *45*). Up to 15 μM *Mt*AhpE failed to inhibit compound I formation from the reaction between HRP (1 μM)

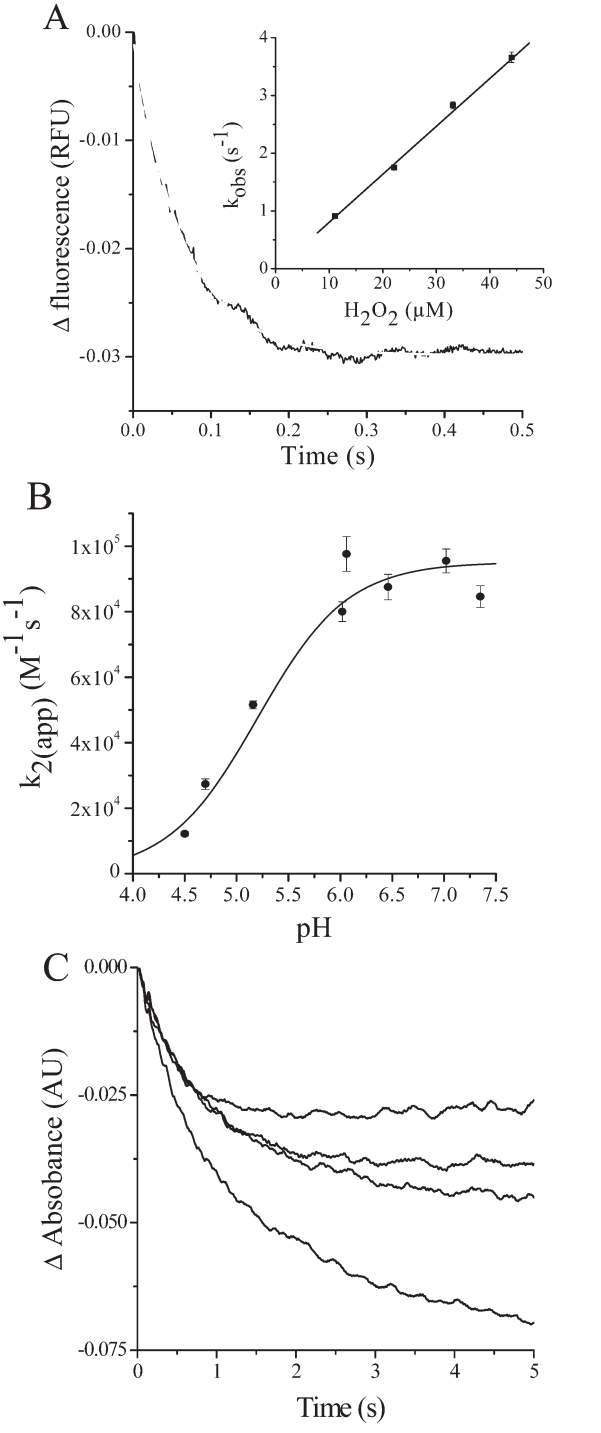

FIGURE 5: Kinetics of H_2O_2-mediated *Mt*AhpE oxidation and peroxidatic thiol pK_a determination. (A) Prereduced *Mt*AhpE (1.0 μM) was rapidly mixed with H_2O_2 (20 μM) in sodium phosphate buffer, 100 mM, containing 0.1 mM dtpa, pH 7.4 and 25 °C, and the time-dependent decrease in total emission fluorescence (λ_{ex} = 280 nm) was followed. The gray trace represents the best fit to a single exponential function. Inset: Effect of increasing H_2O_2 concentrations on the observed rate constants (k_{obs}) of fluorescence change, from which the apparent rate constant of the reaction at pH 7.4 was obtained. (B) Same as in (A) but performed in sodium acetate or sodium phosphate buffers of different pHs as indicated under Materials and Methods. Apparent second-order rate constants for the reaction between reduced enzyme and H_2O_2 obtained (●) were plotted vs pH, and data points were fitted to eq 3 (continuous line). (C) Time courses of LiP (5 μM) oxidation by H_2O_2 (1.0 μM) in the presence of increasing concentrations of reduced *Mt*AhpE (from bottom to top: 0, 3.3, 6.6, and 19.8 μM).

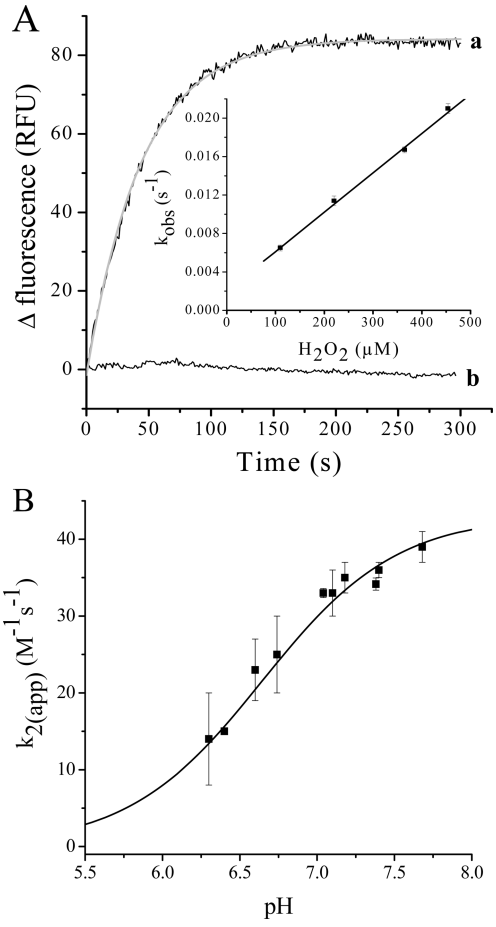

FIGURE 6: Kinetics of H_2O_2-mediated *Mt*AhpE overoxidation and sulfenic acid pK_a determination. (A) Reduced (a) or alkylated (b) *Mt*AhpE (1.0 μM) was mixed with H_2O_2 (230 μM) in sodium phosphate buffer, 100 mM, containing 0.1 mM dtpa, pH 7.4 and 25 °C, and the time-dependent protein fluorescence increase (λ_{ex} = 295 nm, λ_{em} = 338 nm) was determined. The gray trace represents the fit of experimental data in (a) to a single exponential function. Inset: Effect of increasing H_2O_2 concentrations on the observed rate constants (k_{obs}) of fluorescence change, from which the apparent rate constant of the reaction at pH 7.4 was obtained. (B) Same as in (A) but performed in sodium phosphate buffers (100 mM containing 0.1 mM dtpa) of indicated pHs. Apparent second-order rate constants for the reaction between reduced enzyme and H_2O_2 obtained (■) were plotted vs pH, and data points were fitted to eq 3 (continuous line).

and 0.75 μM H_2O_2 (not shown). Since the reaction of H_2O_2 with HRP is 2 orders of magnitude faster than with *Mt*AhpE according to the direct approach, high quantities of *Mt*AhpE (> 100-fold excess over HRP) would be required to inhibit HRP-compound I formation. So, we selected another peroxidase, lignine peroxidase (LiP) (E.C. 1.11.1.14) which is known to react with H_2O_2 to form compound I with a slower rate constant than HRP. The addition of increasing concentrations of reduced *Mt*AhpE produced a dose-dependent inhibition of LiP-compound I formation (Figure 5C). The second-order rate constant for H_2O_2 reduction by *Mt*AhpE was calculated as $(7 \pm 3) \times 10^4$ M^{-1} s^{-1} at pH 7.4 and 25 °C, which is in excellent agreement with the value obtained by the fluorometric approach.

Kinetics of Enzyme Overoxidation by H_2O_2. The kinetics of H_2O_2-mediated *Mt*AhpE overoxidation to sulfinic acid was studied by taking advantage of the increase in intrinsic fluorescence intensity that took place during oxidized *Mt*AhpE exposure to high excess oxidant concentrations, as observed in Figure 1B. Addition of increasing concentrations of H_2O_2 (100−500 μM) caused a dose-dependent increase in the observed rate constants of the intrinsic fluorescence change of *Mt*AhpE (1 μM), and a rate constant of 40 ± 3 M^{-1} s^{-1} at pH 7.4 and 25 °C was determined. The enzyme previously incubated with NEM (5 mM, 30 min) exhibited no significant change in its fluorescence intensity (Figure 6A), that together with the +32 increase in protein molecular weight (Figure 3F) confirmed that the mentioned change was due to C_P overoxidation.

Apparent second-order rate constants of overoxidation were higher at alkaline pHs (Figure 6B), indicating a mechanism of reaction where sulfenate reacted with H_2O_2. The pH-independent rate constant of the reaction was 42 ± 2 M^{-1} s^{-1}. A pK_a value for *Mt*AhpE sulfenic acid of 6.6 ± 0.1 was determined, very similar to the pK_a value previously reported for the sulfenic acid intermediate formed in *Salmonella typhimurium* AhpC, a typical two-cysteine Prx (*56*).

Catalytic Consumption of Hydrogen Peroxide with Thionitrobenzoate as Reductant. When reduced *Mt*AhpE (2.5 μM) and TNB (70 μM) were mixed with H_2O_2 (20 μM), a decrease in TNB concentration was observed (Figure 7A). Under our experimental conditions, and considering the second-order rate constant reported herein, H_2O_2-mediated *Mt*AhpE oxidation to sulfenic acid occurs almost immediately ($t_{1/2}$ = 0. 42 s). Furthermore, the oxidation of TNB by H_2O_2 is negligible (k = 0.45 M^{-1} s^{-1} at pH 7.4 and 25 °C, data not shown). Thus, any decrease in TNB concentration observed would be due to its reaction with oxidized enzyme. Time courses of the reaction were biphasic, with a rapid phase that lasted about 15 s followed by a slower TNB oxidation. Data fitted an exponential plus straight line equation:

$$[\text{TNB}] = A \exp(-k_{obs}t) + St + \text{offset} \quad (4)$$

where A represents the amplitude, k_{obs} is the pseudo-first-order rate constant of the first phase, and S represents the slope of the second phase. The biphasic decay in TNB thus presented typical pre-steady-state kinetics, where the fast consumption of TNB by sulfenic acid (burst) was followed by the rate-limiting turnover of the enzyme. Thus, in addition to reactivity to sulfenic acid to form a mixed disulfide, TNB reacted with the latter, yielding the reduced form of the enzyme which in turn could be again oxidized by H_2O_2 constituting a catalytic cycle:

$$\textit{Mt}\text{AhpE-SH} + H_2O_2 \rightarrow \textit{Mt}\text{AhpE-SOH} + OH^- \text{ (very fast)} \quad (5)$$

$$\textit{Mt}\text{AhpE-SOH} + \text{TNB} \rightarrow \textit{Mt}\text{AhpE-STNB} + OH^- \text{ (fast)} \quad (6)$$

$$\textit{Mt}\text{AhpE-STNB} + \text{TNB} \rightleftharpoons \textit{Mt}\text{AhpE-SH} + \text{DTNB (slow)} \quad (7)$$

The reaction finished after ~60 min, and the total consumption of TNB was twice the concentration of H_2O_2 used, confirming the catalytic mechanism proposed (not shown). The amplitude of the exponential phase was proportional to the enzyme concentration as expected for burst kinetics (Figure 7A, inset) and represented the amount of sulfenic acid that could be detected through mixed disulfide formation in our conditions, 77% of *Mt*AhpE. The rate constant for the reaction of TNB with sulfenic acid (eq 6) was calculated after dividing k_{obs} by [TNB] as $(1.5 \pm 0.3) \times 10^3$ M^{-1} s^{-1} and was independent of the enzyme concentration (data not shown). The rate constant for the reaction between the mixed disulfide and TNB (eq 7) was estimated from the plot of $-(S)$ versus A (i.e., *Mt*AhpE-STNB concentration), after dividing the slope by TNB concentration,

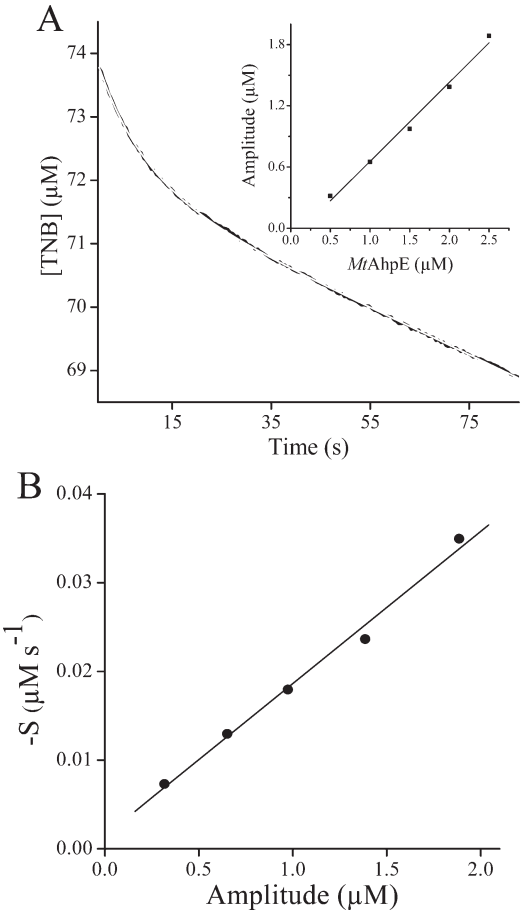

FIGURE 7: Catalytic reduction of *Mt*AhpE by TNB. (A) Reduced *Mt*AhpE (2.5 μM) and TNB (70 μM) in one syringe were mixed with H_2O_2 (20 μM) in the second syringe using a stopped-flow accessory. The decrease in TNB concentration was followed at 412 nm (black trace). The gray trace represents the best fit to eq 4: [TNB] = 1.80 exp(−0.105*t*) − 0.037*t* + 72.03. Inset: Increasing concentrations of *Mt*AhpE were used (0.5−2.5 μM), and the amplitudes of the first phase (A) obtained from eq 4 were plotted against [*Mt*AhpE]. (B) The slopes of the second phase (−*S*), obtained from the fit to eq 4, were plotted against (A).

giving a value of 266 M^{-1} s^{-1} (Figure 7B). Finally, the rate constant of the reaction between reduced *Mt*AhpE and DTNB (reverse of eq 7) was measured as 180 ± 9 M^{-1} s^{-1} at pH 7.4 and 25 °C (not shown).

DISCUSSION

Oxidation of recombinant *Mt*AhpE occurred with a rapid decrease in its fluorescence intensity, which was reverted by DTT (Figure 1A), as well as by the addition of high excess concentrations of the oxidant (Figure 1B). These changes occurred when exciting either at 280 (not shown) or 295 nm (Figure 1A,B), indicating that at least one of the three tryptophan residues present in the protein sequence is involved in the process. Changes in fluorescence intensity pointed toward structural modifications of the protein under different redox states, which caused differential quenching of tryptophan fluorescence by neighboring, not yet identified, amino acid residues (*57*). Reduced *Mt*AhpE was a noncovalent dimer in solution and oligomerized upon treatment with equimolar concentrations of H_2O_2. These changes in quaternary structure were much slower and thus were not responsible for the fluorescence intensity decrease (Figure 2A) and were reverted by protein reduction (Figure 2B). Oligomerization did not occur when the enzyme was exposed to high excess oxidant concentrations that caused overoxidation (Figure 2A). These data are consistent with the reported crystallography structure of *Mt*AhpE, that evidenced important differences in conformation at reduced versus oxidized states[4] (*24*). Although the structure of the overoxidized form of the enzyme is not available, our data suggest that reduced and overoxidized forms of *Mt*AhpE have similar conformations, as reported for 2-Cys Prxs (*36*). Oxidation of the thiol by equimolar peroxide concentrations led to sulfenic acid formation, that was trapped by GSH, NAC, and TNB leading to mixed disulfide formation (Figures 3D,E and 7A) and that was reduced by DTT and TNB (Figures 3C and 7B). This is in agreement with crystallography data which showed that the cysteine residue was oxidized to sulfenic acid in the oxidized form of the enzyme (*24*) and with our results indicating that only a slight fraction of the enzyme formed intermolecular disulfides upon oxidation.

The fact that the observed rate constant of fluorescence decrease showed a linear relationship with oxidant concentration indicated that oxidation was rate-limiting the overall process leading to changes in fluorescent intensity (Figures 4A and 5A). This was confirmed by using alternative approaches based on competition kinetics that yielded very similar *k* values (Figure 4A versus Figure 4B; Figure 5A versus Figure 5C). As in the case of human Prx5, but contrary to what we observed for human red blood cell Prx2, or was reported for mammal Prx 6, bacterial AhpC, or yeast TSA1 and TSA2, peroxynitrite-mediated *Mt*AhpE oxidation was at least 2 orders of magnitude faster than that mediated by H_2O_2 (Table 1), indicating that the enzyme is a highly selective peroxidase. In general, kinetics of reactions of low molecular weight thiols with different peroxides follow the trend indicated by Edwards; i.e., those peroxides with the lower pK_a of the leaving group react faster than the others (*58*). The trend appears to be maintained in the case of *Mt*AhpE C_P, at least for the peroxides tested so far. However, it is lost in many Prxs (*46*). Thus, the molecular basis for oxidizing substrate specificity in Prxs is intriguing, and its rationalization will require a thorough combined analysis of kinetic and structural data for Prxs of different subfamilies.

Thiolates are known to be the nucleophile species during peroxide reduction, and therefore peroxidatic thiol pK_a could affect this reactivity. In the case of *Mt*AhpE this was 5.2 (Figure 4B), being the first determination for a 1-Cys Prx. A low pK_a value indicates that the thiol would be almost totally in its reactive form at pHs the enzyme is expected to encounter *in vivo*. This value is similar to those reported for other, 2-cys Prxs (< 5−6.3 (*59*)), in agreement with the similar active site geometry.

*Mt*AhpE catalytic activity requires sulfenic acid reduction. Oxidized *Mt*AhpE formed mixed disulfides with different monothiols tested (Figure 3D,E). For selected 1-Cys Prxs, mixed disulfide formation with GSH and their reduction have been reported (*29*, *30*, *32*). However, Mycobacteria lack glutathione and contain a particular set of low molecular weight thiols (*10*) and thiol−disulfide reductases (*13*), and evidence for enzymatic routes for *Mt*AhpE-mixed disulfide reduction is lacking so far. Although we did not identify potential natural reducing substrates for the enzyme, we succeeded in designing a spectrophotometric

[4]Although the crystal structure of reduced enzyme reported was composed by two asymmetric dimers (*24*), for which we found no evidence in our gel filtration experiments, this probably reflects different experimental conditions and/or labile enzyme dimer association.

Table 1: Kinetics of H_2O_2 and Peroxynitrite Reduction by Peroxiredoxins[a]

Prx	Prx type	$k_{2\,H_2O_2}$ (M^{-1} s^{-1})	$k_{2\,ONOOH}$ (M^{-1} s^{-1})	ref
S. typhimurium AhpC	typical 2-Cys	4×10^{7} [b]		*65*
			1.5×10^{6} [c]	*62*
M. tuberculosis AhpE	1-Cys	8.2×10^{4}	1.9×10^{7}	this work
M. tuberculosis TPx	atypical 2-Cys	ND	1.5×10^{7}	*9*
H. sapiens Prx 2	typical 2-Cys	1.3×10^{7}		*45*
		1.0×10^{8}	1.4×10^{7}	*47*
H. sapiens Prx 5	atypical 2-Cys		7×10^{7} [d]	*67*
		3×10^{5}	6.7×10^{7} [d]	*46*
S. cerevisiae Tsa1	typical 2-Cys	2.2×10^{7}	7.4×10^{5}	*68*
S. cerevisiae Tsa2	typical 2-Cys	1.3×10^{7}	5.1×10^{5}	*68*

[a]Rate constants were reported at pH 7.4 and 25 °C unless otherwise indicated. ND is not determined. [b]At pH 7. [c]At pH 6.75, a similar value was reported for peroxynitrite reduction by *M. tuberculosis* AhpC (*62*). [d]At pH 7.8.

method for easily measuring catalytic activity using the artificial reductant TNB. This reagent also allowed detecting and quantifying sulfenic acid in oxidized *Mt*AhpE (Figure 7).

As above-mentioned, excess H_2O_2 led to a rapid decrease followed by a slower increase in *Mt*AhpE fluorescence intensity that were precluded by thiol alkylation (Figures 1B and 6A). The observed rate constant of the second phase was linearly dependent on H_2O_2 concentration, again indicating that the bimolecular reaction was the rate-limiting step of the process (Figure 6A), and a +32 molecular weight increase was detected (Figure 3F). Altogether, these data are indicative of H_2O_2-mediated thiol overoxidation to sulfinic acid with a rate constant of 40 ± 3 M^{-1} s^{-1} at pH 7.4 and 25 °C. This value is very similar to the 57 M^{-1} s^{-1} calculated previously for Prx 1 inactivation (*35*, *36*) and much faster than reported rate constants for H_2O_2-mediated oxidation of sulfenic acid in human serum albumin or streptococcal NADH peroxidase ($k = 0.4 \pm 0.2$ M^{-1} s^{-1} and 0.14 M^{-1} s^{-1}, respectively (*39*, *60*)). Moreover, rate constants of H_2O_2-mediated sulfenic acid oxidation were faster at alkaline pH, consistent with a mechanism of reaction where sulfenate is the reactive species, suggesting nucleophilic attack on the peroxidic oxygen (followed by rearrangement to sulfinic acid). The pH profile for this reaction allowed us to calculate the pK_a of the sulfenic acid at the oxidized enzyme as 6.6 ± 0.1 (Figure 6B), very similar to the reported pK_a (=6.1) of the sulfenic acid intermediate formed during peroxidatic thiol oxidation in the bacterial 2-Cys Prx AhpC (*56*). Since the intrabacterial pH of wild-type *M. tuberculosis* inside both nonactivated and IFN-γ-activated macrophages has been reported as 6.8−7.5 (*61*), >95% thiol and >50% sulfenic acid would be deprotonated and therefore, at their reactive form with peroxides, in reduced and oxidized *Mt*AhpE, respectively. Oxidative inactivation susceptibility is dictated by the competition between two processes: sulfenic acid oxidation to sulfinic acid vs its resolution. Our data give experimental support to the idea originally proposed by Wood et al. (*36*), indicating that rates of sulfenic acid oxidation are similar for different Prxs and that susceptibility to inactivation by overoxidation depends mainly in different rates of sulfenic acid reaction with the resolving thiol or substrate(s).

In conclusion, this work contributes to the functional characterization of the one-cysteine Prx codified in the genome of *M. tuberculosis*, *Mt*AhpE, for which evidence of expression already exists at a transcriptional level (*23*). Its rapid reaction with peroxynitrite, which resulted as fast as with *Mt*TPx and 10-fold faster than with catalase peroxidase (*9*, *15*, *62*), suggests that *Mt*AhpE represents an important antioxidant defense against this cytotoxic molecule, which can be formed by activated macrophages during infection (*63*). On the contrary, other *M. tuberculosis* enzymes, especially *Mt*AhpC and catalase peroxidase, reduced H_2O_2 with a greater rate constant than *Mt*AhpE (*64*, *65*). However, it is important to consider at this point that preferential routes for peroxide reduction would be dictated not only by the rate constant, k, but by rates of reaction ($k \times$ [target]). Concentrations of these enzymes are mostly unknown in *M. tuberculosis* and may change depending on different conditions (*66*). Thus, our *in vitro* data provide kinetic evidence indicating that *Mt*AhpE could play a role for selected cytotoxic peroxide detoxification, especially peroxynitrite, but further investigation will be required to understand its role in *M. tuberculosis* pathobiology. In this regard, it should be noted that although peroxidatic active site structure is conserved among different Prxs, *Mt*AhpE structure differs in some aspects from Prxs present in mammal cells (*24*). Therefore, its functional and structural characterization is not only an important step toward the understanding the bacterial mechanisms of antioxidant defense but could also facilitate future investigation regarding its validation as a potential drug target for the treatment of the tuberculosis disease.

ACKNOWLEDGMENT

We thank Dr. Pedro Alzari from Institut Pasteur Paris, France, for kindly providing the plasmid of His-tag *Mt*AhpE and Dr. Gonzalo Peluffo from Universidad de la República, Uruguay, for assistance in mass spectrometry determinations.

REFERENCES

1. WHO Report (2009) Global Tuberculosis Control: Epidemiology, Strategy, Financing, pp 6−33, World Health Organization.
2. Zahrt, T. C., and Deretic, V. (2002) Reactive nitrogen and oxygen intermediates and bacterial defenses: unusual adaptations in *Mycobacterium tuberculosis*. *Antioxid. Redox Signaling 4*, 141–159.
3. Fang, F. C. (2004) Antimicrobial reactive oxygen and nitrogen species: concepts and controversies. *Nat. Rev. Microbiol. 2*, 820–832.
4. Nathan, C., and Shiloh, M. U. (2000) Reactive oxygen and nitrogen intermediates in the relationship between mammalian hosts and microbial pathogens. *Proc. Natl. Acad. Sci. U.S.A. 97*, 8841–8848.
5. Shiloh, M. U., and Nathan, C. F. (2000) Reactive nitrogen intermediates and the pathogenesis of *Salmonella* and mycobacteria. *Curr. Opin. Microbiol. 3*, 35–42.
6. MacMicking, J. D., North, R. J., LaCourse, R., Mudgett, J. S., Shah, S. K., and Nathan, C. F. (1997) Identification of nitric oxide synthase as a protective locus against tuberculosis. *Proc. Natl. Acad. Sci. U.S.A. 94*, 5243–5248.
7. Nozaki, Y., Hasegawa, Y., Ichiyama, S., Nakashima, I., and Shimokata, K. (1997) Mechanism of nitric oxide-dependent killing of *Mycobacterium bovis* BCG in human alveolar macrophages. *Infect. Immun. 65*, 3644–3647.
8. Manca, C., Paul, S., Barry, C. E.III, Freedman, V. H., and Kaplan, G. (1999) *Mycobacterium tuberculosis* catalase and peroxidase activities

and resistance to oxidative killing in human monocytes in vitro. *Infect. Immun. 67*, 74–79.
9. Jaeger, T., Budde, H., Flohe, L., Menge, U., Singh, M., Trujillo, M., and Radi, R. (2004) Multiple thioredoxin-mediated routes to detoxify hydroperoxides in *Mycobacterium tuberculosis*. *Arch. Biochem. Biophys. 423*, 182–191.
10. Newton, G. L., Arnold, K., Price, M. S., Sherrill, C., Delcardayre, S. B., Aharonowitz, Y., Cohen, G., Davies, J., Fahey, R. C., and Davis, C. (1996) Distribution of thiols in microorganisms: mycothiol is a major thiol in most actinomycetes. *J. Bacteriol. 178*, 1990–1995.
11. Patel, M. P., and Blanchard, J. S. (1999) Expression, purification, and characterization of *Mycobacterium tuberculosis* mycothione reductase. *Biochemistry 38*, 11827–11833.
12. Ordonez, E., Van Belle, K., Roos, G., De Galan, S., Letek, M., Gil, J. A., Wyns, L., Mateos, L. M., and Messens, J. (2009) Arsenate reductase, mycothiol, and mycoredoxin concert thiol/disulfide exchange. *J. Biol. Chem. 284*, 15107–15116.
13. den Hengst, C. D., and Buttner, M. J. (2008) Redox control in actinobacteria. *Biochim. Biophys. Acta 1780*, 1201–1216.
14. Timmins, G. S., and Deretic, V. (2006) Mechanisms of action of isoniazid. *Mol. Microbiol. 62*, 1220–1227.
15. Wengenack, N. L., Jensen, M. P., Rusnak, F., and Stern, M. K. (1999) *Mycobacterium tuberculosis* KatG is a peroxynitritase. *Biochem. Biophys. Res. Commun. 256*, 485–487.
16. Wengenack, N. L., and Rusnak, F. (2001) Evidence for isoniazid-dependent free radical generation catalyzed by *Mycobacterium tuberculosis* KatG and the isoniazid-resistant mutant KatG(S315T). *Biochemistry 40*, 8990–8996.
17. Sherman, D. R., Mdluli, K., Hickey, M. J., Arain, T. M., Morris, S. L., Barry, C. E., and Stover, C. K. (1996) Compensatory ahpC gene expression in isoniazid-resistant *Mycobacterium tuberculosis*. *Science 272*, 1641–1643.
18. Hu, Y., and Coates, A. R. (2009) Acute and persistent *Mycobacterium tuberculosis* infections depend on the thiol peroxidase TpX. *PLoS ONE 4*, e5150.
19. Cole, S. T., Brosch, R., Parkhill, J., Garnier, T., Churcher, C., Harris, D., Gordon, S. V., Eiglmeier, K., Gas, S., Barry, C. E., Tekaia, F., Badcock, K., Basham, D., Brown, D., Chillingworth, T., Connor, R., Davies, R., Devlin, K., Feltwell, T., Gentles, S., Hamlin, N., Holroyd, S., Hornsby, T., Jagels, K., Krogh, A., McLean, J., Moule, S., Murphy, L., Oliver, K., Osborne, J., Quail, M. A., Rajandream, M. A., Rogers, J., Rutter, S., Seeger, K., Skelton, J., Squares, Squares, S., Sulston, J. E., Taylor, K., Whitehead, S., and Barrell, B. G. (1998) Deciphering the biology of *Mycobacterium tuberculosis* from the complete genome sequence. *Nature 393*, 537–544.
20. Kang, G. Y., Park, E. H., Kim, K., and Lim, C. J. (2009) Overexpression of bacterioferritin comigratory protein (Bcp) enhances viability and reduced glutathione level in the fission yeast under stress. *J. Microbiol. 47*, 60–67.
21. Limauro, D., Pedone, E., Galdi, I., and Bartolucci, S. (2008) Peroxiredoxins as cellular guardians in *Sulfolobus solfataricus*: characterization of Bcp1, Bcp3 and Bcp4. *FEBS J. 275*, 2067–2077.
22. Passardi, F., Theiler, G., Zamocky, M., Cosio, C., Rouhier, N., Teixera, F., Margis-Pinheiro, M., Ioannidis, V., Penel, C., Falquet, L., and Dunand, C. (2007) PeroxiBase: the peroxidase database. *Phytochemistry 68*, 1605–1611.
23. Murphy, D. J., and Brown, J. R. (2007) Identification of gene targets against dormant phase *Mycobacterium tuberculosis* infections. *BMC Infect. Dis. 7*, 84.
24. Li, S., Peterson, N. A., Kim, M. Y., Kim, C. Y., Hung, L. W., Yu, M., Lekin, T., Segelke, B. W., Lott, J. S., and Baker, E. N. (2005) Crystal structure of AhpE from *Mycobacterium tuberculosis*, a 1-Cys peroxiredoxin. *J. Mol. Biol. 346*, 1035–1046.
25. Wood, Z. A., Poole, L. B., Hantgan, R. R., and Karplus, P. A. (2002) Dimers to doughnuts: redox-sensitive oligomerization of 2-cysteine peroxiredoxins. *Biochemistry 41*, 5493–5504.
26. Poole, L. B. (2007) The catalytic mechanism of peroxiredoxins. *Subcell. Biochem. 44*, 61–81.
27. Choi, H. J., Kang, S. W., Yang, C. H., Rhee, S. G., and Ryu, S. E. (1998) Crystal structure of a novel human peroxidase enzyme at 2.0 Å resolution. *Nat. Struct. Biol. 5*, 400–406.
28. Rhee, S. G., Chae, H. Z., and Kim, K. (2005) Peroxiredoxins: a historical overview and speculative preview of novel mechanisms and emerging concepts in cell signaling. *Free Radical Biol. Med. 38*, 1543–1552.
29. Ralat, L. A., Manevich, Y., Fisher, A. B., and Colman, R. F. (2006) Direct evidence for the formation of a complex between 1-cysteine peroxiredoxin and glutathione S-transferase pi with activity changes in both enzymes. *Biochemistry 45*, 360–372.
30. Ralat, L. A., Misquitta, S. A., Manevich, Y., Fisher, A. B., and Colman, R. F. (2008) Characterization of the complex of glutathione *S*-transferase pi and 1-cysteine peroxiredoxin. *Arch. Biochem. Biophys. 474*, 109–118.
31. Monteiro, G., Horta, B. B., Pimenta, D. C., Augusto, O., and Netto, L. E. (2007) Reduction of 1-Cys peroxiredoxins by ascorbate changes the thiol-specific antioxidant paradigm, revealing another function of vitamin C. *Proc. Natl. Acad. Sci. U.S.A. 104*, 4886–4891.
32. Greetham, D., and Grant, C. M. (2009) Antioxidant activity of the yeast mitochondrial one-Cys peroxiredoxin is dependent on thioredoxin reductase and glutathione in vivo. *Mol. Cell. Biol. 29*, 3229–3240.
33. Pedrajas, J. R., Miranda-Vizuete, A., Javanmardy, N., Gustafsson, J. A., and Spyrou, G. (2000) Mitochondria of *Saccharomyces cerevisiae* contain one-conserved cysteine type peroxiredoxin with thioredoxin peroxidase activity. *J. Biol. Chem. 275*, 16296–16301.
34. Kim, S. Y., Jo, H. Y., Kim, M. H., Cha, Y. Y., Choi, S. W., Shim, J. H., Kim, T. J., and Lee, K. Y. (2008) H_2O_2-dependent hyperoxidation of peroxiredoxin 6 (Prdx6) plays a role in cellular toxicity via up-regulation of iPLA2 activity. *J. Biol. Chem. 283*, 33563–33568.
35. Stone, J. R. (2004) An assessment of proposed mechanisms for sensing hydrogen peroxide in mammalian systems. *Arch. Biochem. Biophys. 422*, 119–124.
36. Wood, Z. A., Poole, L. B., and Karplus, P. A. (2003) Peroxiredoxin evolution and the regulation of hydrogen peroxide signaling. *Science 300*, 650–653.
37. Beckman, J. S., Beckman, T. W., Chen, J., Marshall, P. A., and Freeman, B. A. (1990) Apparent hydroxyl radical production by peroxynitrite: implications for endothelial injury from nitric oxide and superoxide. *Proc. Natl. Acad. Sci. U.S.A. 87*, 1620–1624.
38. Radi, R., Beckman, J. S., Bush, K. M., and Freeman, B. A. (1991) Peroxynitrite oxidation of sulfhydryls. The cytotoxic potential of superoxide and nitric oxide. *J. Biol. Chem. 266*, 4244–4250.
39. Turell, L., Botti, H., Carballal, S., Ferrer-Sueta, G., Souza, J. M., Duran, R., Freeman, B. A., Radi, R., and Alvarez, B. (2008) Reactivity of sulfenic acid in human serum albumin. *Biochemistry 47*, 358–367.
40. Claiborne, A., Miller, H., Parsonage, D., and Ross, R. P. (1993) Protein-sulfenic acid stabilization and function in enzyme catalysis and gene regulation. *FASEB J. 7*, 1483–1490.
41. Pace, C. N., Vajdos, F., Fee, L., Grimsley, G., and Gray, T. (1995) How to measure and predict the molar absorption coefficient of a protein. *Protein Sci. 4*, 2411–2423.
42. Schonbaum, G. R., and Lo, S. (1972) Interaction of peroxidases with aromatic peracids and alkyl peroxides. Product analysis. *J. Biol. Chem. 247*, 3353–3360.
43. Tien, M., Kirk, T. K., Bull, C., and Fee, J. A. (1986) Steady-state and transient-state kinetic studies on the oxidation of 3,4-dimethoxybenzyl alcohol catalyzed by the ligninase of *Phanerocheate chrysosporium* Burds. *J. Biol. Chem. 261*, 1687–1693.
44. Ogusucu, R., Rettori, D., Munhoz, D. C., Netto, L. E., and Augusto, O. (2007) Reactions of yeast thioredoxin peroxidases I and II with hydrogen peroxide and peroxynitrite: rate constants by competitive kinetics. *Free Radical Biol. Med. 42*, 326–334.
45. Peskin, A. V., Low, F. M., Paton, L. N., Maghzal, G. J., Hampton, M. B., and Winterbourn, C. C. (2007) The high reactivity of peroxiredoxin 2 with H(2)O(2) is not reflected in its reaction with other oxidants and thiol reagents. *J. Biol. Chem. 282*, 11885–11892.
46. Trujillo, M., Clippe, A., Manta, B., Ferrer-Sueta, G., Smeets, A., Declercq, J. P., Knoops, B., and Radi, R. (2007) Pre-steady state kinetic characterization of human peroxiredoxin 5: taking advantage of Trp84 fluorescence increase upon oxidation. *Arch. Biochem. Biophys. 467*, 95–106.
47. Manta, B., Hugo, M., Ortiz, C., Ferrer-Sueta, G., Trujillo, M., and Denicola, A. (2008) The peroxidase and peroxynitrite reductase activity of human erythrocyte peroxiredoxin 2. *Arch. Biochem. Biophys. 484*, 146–154.
48. Hayashi, Y., and Yamazaki, I. (1979) The oxidation-reduction potentials of compound I/compound II and compound II/ferric couples of horseradish peroxidases A2 and C. *J. Biol. Chem. 254*, 9101–9106.
49. Floris, R., Piersma, S. R., Yang, G., Jones, P., and Wever, R. (1993) Interaction of myeloperoxidase with peroxynitrite. A comparison with lactoperoxidase, horseradish peroxidase and catalase. *Eur. J. Biochem. 215*, 767–775.
50. Mendes, P. (1993) GEPASI: a software package for modelling the dynamics, steady states and control of biochemical and other systems. *Comput. Appl. Biosci. 9*, 563–571.
51. Mendes, P. (1997) Biochemistry by numbers: simulation of biochemical pathways with Gepasi 3. *Trends Biochem. Sci. 22*, 361–363.

52. Peshenko, I. V., and Shichi, H. (2001) Oxidation of active center cysteine of bovine 1-Cys peroxiredoxin to the cysteine sulfenic acid form by peroxide and peroxynitrite. *Free Radical Biol. Med. 31*, 292–303.
53. Steffek, M., Newton, G. L., Av-Gay, Y., and Fahey, R. C. (2003) Characterization of *Mycobacterium tuberculosis* mycothiol S-conjugate amidase. *Biochemistry 42*, 12067–12076.
54. Hofmann, B., Hecht, H. J., and Flohe, L. (2002) Peroxiredoxins. *Biol. Chem. 383*, 347–364.
55. Wood, Z. A., Schroder, E., Harris, R. J., and Poole, L. B. (2003) Structure, mechanism and regulation of peroxiredoxins. *Trends Biochem. Sci. 28*, 32–40.
56. Poole, L. B., and Ellis, H. R. (2002) Identification of cysteine sulfenic acid in AhpC of alkyl hydroperoxide reductase. *Methods Enzymol. 348*, 122–136.
57. Lakowicz, J. R. (1999) Principles of Fluorescence Spectroscopy , 2nd ed.; Springer: New York.
58. Edwards, J. O. (1962) Nucleophilic displacement on oxygen in peroxides, in Peroxide Reaction Mechanisms (Edwards, J. O., Ed.) pp 67−106, Interscience, New York.
59. Trujillo, M., Ferrer-Sueta, G., and Radi, R. (2008) Peroxynitrite detoxification and its biologic implications. *Antioxid. Redox Signaling 10*, 1607–1620.
60. Poole, L. B., and Claiborne, A. (1989) The non-flavin redox center of the streptococcal NADH peroxidase. II. Evidence for a stabilized cysteine-sulfenic acid. *J. Biol. Chem. 264*, 12330–12338.
61. Vandal, O. H., Pierini, L. M., Schnappinger, D., Nathan, C. F., and Ehrt, S (2008) A membrane protein preserves intrabacterial pH in intraphagosomal *Mycobacterium tuberculosis*. *Nat. Med. 14*, 849–854.
62. Bryk, R., Griffin, P., and Nathan, C. (2000) Peroxynitrite reductase activity of bacterial peroxiredoxins. *Nature 407*, 211–215.
63. Alvarez, M. N., Piacenza, L., Irigoin, F., Peluffo, G., and Radi, R. (2004) Macrophage-derived peroxynitrite diffusion and toxicity to *Trypanosoma cruzi*. *Arch. Biochem. Biophys. 432*, 222–232.
64. Jakopitsch, C., Vlasits, J., Wiseman, B., Loewen, P. C., and Obinger, C. (2007) Redox intermediates in the catalase cycle of catalase-peroxidases from *Synechocystis* PCC 6803, *Burkholderia pseudomallei*, and *Mycobacterium tuberculosis*. *Biochemistry 46*, 1183–1193.
65. Parsonage, D., Karplus, P. A., and Poole, L. B. (2008) Substrate specificity and redox potential of AhpC, a bacterial peroxiredoxin. *Proc. Natl. Acad. Sci. U.S.A. 105*, 8209–8214.
66. Springer, B., Master, S., Sander, P., Zahrt, T., McFalone, M., Song, J., Papavinasasundaram, K. G., Boettger, E., and Deretic, V. (2001) Silencing of oxidative stress response in *Mycobacterium tuberculosis*: expression patterns of ahpC in virulent and avirulent strains and effect of ahpC inactivation. *Infect. Immun. 69*, 5967–5973.
67. Dubuisson, M., Vander Stricht, D., Clippe, A., Etienne, F., Nauser, T., Kissner, R., Koppenol, W. H., Rees, J. F., and Knoops, B. (2004) Human peroxiredoxin 5 is a peroxynitrite reductase. *FEBS Lett. 571*, 161–165.
68. Ogusucu, R., Rettori, D., Munhoz, D. C., Netto, L. E., and Augusto, O. (2007) Reactions of yeast thioredoxin peroxidases I and II with hydrogen peroxide and peroxynitrite: rate constants by competitive kinetics. *Free Radical Biol. Med. 42*, 326–334.